Supplementary information

Visualizing Hydrogen Nanobubbles Generation at Nanoscale Zero-valent Iron/Water Interfaces

Shuangjia Shi[a], Qing Huang[*a, b, c], Wei-xian Zhang[a], Lijuan Zhang[*b, d, e], Airong Liu[*a]

[a]State Key Laboratory of Water Pollution Control and Green Resource Recycling, College of Environmental Science and Engineering, Tongji University, Shanghai 200092, China

[b]Shanghai Synchrotron Radiation Facility, Shanghai Advanced Research Institute, Chinese Academy of Sciences, Shanghai 201204, China

[c]Faculty of Chemical Engineering and Energy Technology, Shanghai Institute of Technology, Shanghai 201418, China

[d]University of the Chinese Academy of Sciences, Beijing 100049, China

[e]Shanghai Institute of Applied Physics, Chinese Academy of Sciences, Shanghai 201800, China

*Author to whom correspondence should be addressed
Airong Liu, Email: liuairong@tongji.edu.cn ; Lijuan Zhang, Email: zhanglijuan@sari.ac.cn; Qing Huang, Email: hq@sit.edu.cn

Text S1. Chemicals and reagents

Ferric chloride hexahydrate ($FeCl_3 \cdot 6H_2O$, AR) and sodium borohydride ($NaBH_4$, AR) were purchased from Sigma Aldrich (Shanghai, China) Trading Co., Ltd. Absolute ethanol (EtOH, AR) was obtained from Sinopharm Chemical Reagent Co., Ltd. (Shanghai, China). All aqueous solutions were prepared using deionized water. High-purity nitrogen gas (>99.9%) was supplied by Shanghai Wendong Gas Co., Ltd. and used for solution deoxygenation and to maintain anaerobic conditions during sample handling.

Chemicals used for nanobubble visualization and supporting measurements were all analytical grade unless otherwise noted. For AFM substrate preparation, freshly cleaved highly oriented pyrolytic graphite (HOPG, grade ZYB; Beijing Scistar Technology Co., Ltd.) was used. Spin-trapping experiments for EPR employed 5,5-dimethyl-1-pyrroline N-oxide (DMPO, ≥99%, Sigma Aldrich). Electrochemical measurements utilized sodium sulfate (Na_2SO_4, AR; Sinopharm Chemical Reagent Co., Ltd.) as the electrolyte and Nafion solution (5 wt%, Sigma Aldrich) as the binder for electrode fabrication. For NTA, samples were filtered using 0.22 μm polyethersulfone (PES) syringe filters (Anpu Laboratory Equipment Co., Ltd.). All other routine reagents—including acids, bases, and standard laboratory solvents used for cleaning, washing, or preparing stock solutions—were purchased from Sinopharm Chemical Reagent Co., Ltd. and used as received without additional purification.

Text S2. Synthesis of nZVI.

nZVI was synthesized using a liquid-phase reduction method. Briefly, a $NaBH_4$ solution (0.2 mol·L^{-1}) was added dropwise (1:1 volume ratio) to a $FeCl_3 \cdot 6H_2O$ solution (0.05 mol·L^{-1}) at room temperature under a nitrogen atmosphere with continuous stirring, leading to rapid reduction as shown in Equation (1). The resulting black precipitates were allowed to settle, magnetically separated, and rinsed three times with deionized water and absolute ethanol. The purified nanoparticles were then stored in 99.8% ethanol in sealed polyethylene bottles at 4 °C prior to use.

$$4Fe^{3+} + 3BH_4^- + 9H_2O \rightarrow 4Fe^0\downarrow + 3H_2BO_3^- + 12H^+$$

Text S3. NTA workflow for quantification of HNBs

NTA was used to quantify the size distribution and number concentration of nanoscale entities generated during nZVI corrosion and attributed to hydrogen nanobubbles. As illustrated in **Fig. S1**, individual scattering centers were tracked under laser illumination and their Brownian motion trajectories were analyzed to obtain diffusion coefficients, which were then converted to hydrodynamic diameters using the Stokes–Einstein equation. [1-3] Measurements were conducted at 25 °C with an instrument sensitivity of 65 and a shutter value of 150.For each condition, nZVI suspensions (0, 50, 100, 150, 200 and 400 mg L^{-1}) were reacted in deionized water for 120 min and subsequently filtered through 0.22 μm membranes prior to NTA analysis to minimize interference from residual solid particles.. Ethanol-based nZVI suspensions at the same loadings analyzed in parallel as controls. Where indicated, aqueous filtrates were further subjected to freeze–vacuum degassing before NTA measurement. The resulting filtrates were introduced into the measurement chamber for video acquisition, particle tracking, and trajectory reconstruction. Representative videos are provided **in Video S1**. The displayed NTA frames represent algorithm-detected scattering centers rather than the true morphology of individual nanobubbles.

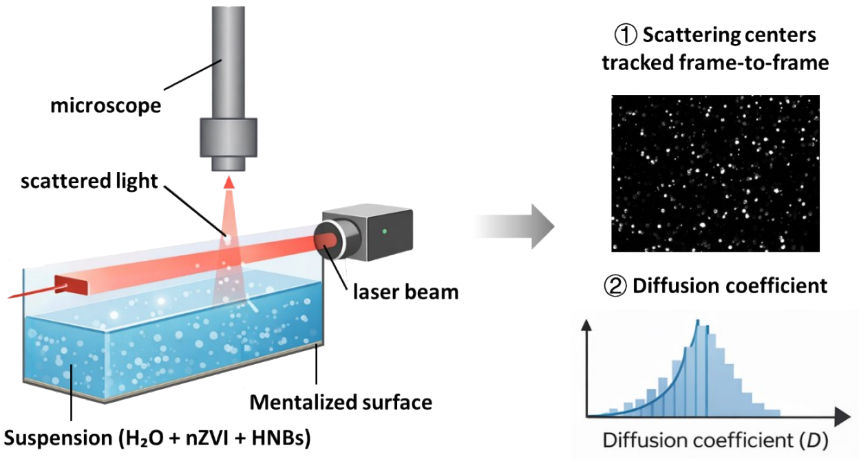

Figure S1. NTA workflow for quantifying nanoscale scatterers attributed to hydrogen nanobubbles in nZVI reaction filtrates.

Text S4. Principles and workflow of in-situ STXM imaging

STXM was used to generate nanoscale optical-density maps by raster-scanning a focused, monochromatic soft X-ray probe across the sample while recording the transmitted intensity with a downstream detector (schematic **in Fig. S2**). Imaging was conducted at the oxygen K-edge (540 eV), where strong absorption by water yields high contrast such that gas-filled domains appear as high-transmission, low-density features relative to the surrounding liquid. [4, 5] Leveraging sub-30 nm spatial resolution together with energy-selective contrast, STXM enables direct in-liquid visualization of interfacial gas domains within confined liquid environments.

To capture the rapid formation of HNBs during nZVI corrosion, two suspensions were prepared immediately before imaging: nZVI dispersed in ethanol (control) and in deionized water (experimental), each diluted to 2 mg L^{-1}. Approximately 0.50 μL of suspension was sandwiched between two Si_3N_4 membranes mounted on an STXM-compatible holder, and the window perimeter was sealed with vacuum grease to minimize evaporation and gas exchange; blank Si_3N_4 membranes were prepared in the same manner. The assembled liquid cell was transferred into the STXM chamber and evacuated to ~10^{-6} Torr. Before data acquisition, optical microscopy was used to confirm continuous interference fringes, indicating a uniform liquid film (~2–5 μm) suitable for soft X-ray transmission. STXM images were then acquired at 540 eV to resolve water–gas contrast under ambient temperature.

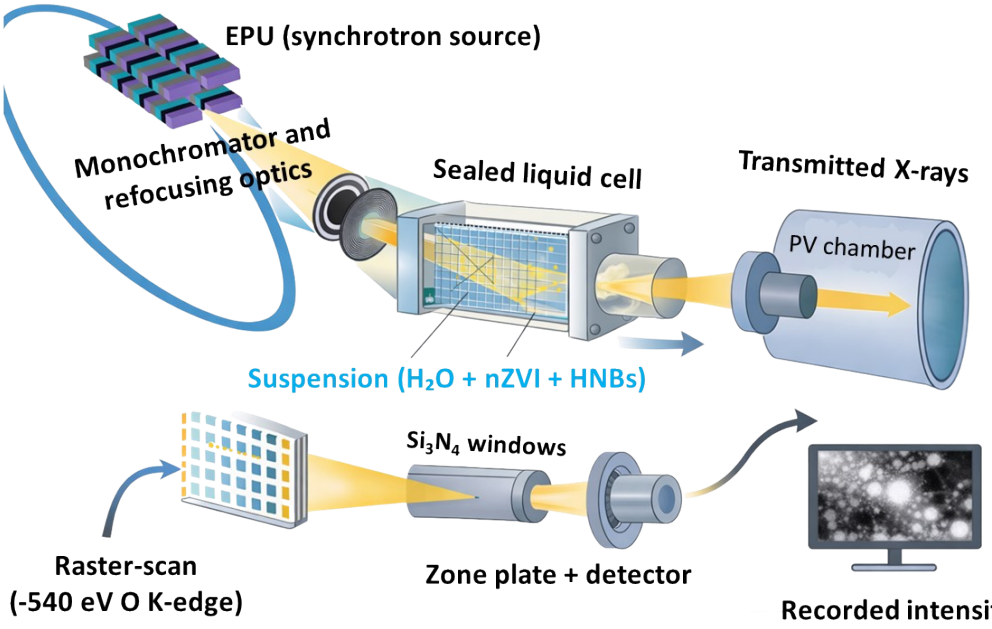

Figure S2. Schematic illustration of in-liquid STXM imaging for visualizing hydrogen nanobubbles.

Text S5. AFM workflow for in-Liquid nanobubble visualization

AFM was employed to resolve nanoscale interfacial structures emerging during the reaction between nZVI and water (**Fig. S3**). AFM detects interaction forces between a sharp probe mounted on a microcantilever and the sample surface, enabling quantitative mapping of surface topography and local nanomechanical properties with near-atomic spatial resolution. [6]

For sample preparation, a dilute ethanol suspension of nZVI was drop-cast onto freshly cleaved highly oriented pyrolytic graphite (HOPG) and dried under a nitrogen atmosphere. The substrate was then mounted into a sealed liquid cell equipped with a replaceable O-ring, allowing controlled fluid exchange while maintaining mechanical stability. Baseline imaging of nZVI particles was first performed in air using PeakForce quantitative nanomechanical (PF-QNM) mode (scan rate: 0.997 Hz; peak-force frequency: 2 kHz; resolution: 256 × 256 pixels) to establish initial topographic and mechanical references.

To initiate corrosion, deeply degassed degassed deionized water (DIW) was introduced into the sealed fluid cell. Degassing was achieved by three freeze–pump–thaw cycles (freezing at −20 °C, evacuation to 0.1 atm for 10 h, followed by refreezing), ensuring effective removal of pre-existing dissolved gases. Upon contact with DIW, surface-bound nZVI underwent immediate interfacial reactions. Time-resolved PF-QNM imaging was subsequently performed in situ to capture the emergence and evolution of nanoscale gas domains. Emerging features exhibiting markedly lower stiffness and distinct phase contrast relative to the surrounding solid particles were identified as nanobubble domains, allowing AFM to distinguish mechanically compliant nanobubble-related features from solid iron particles during corrosion.

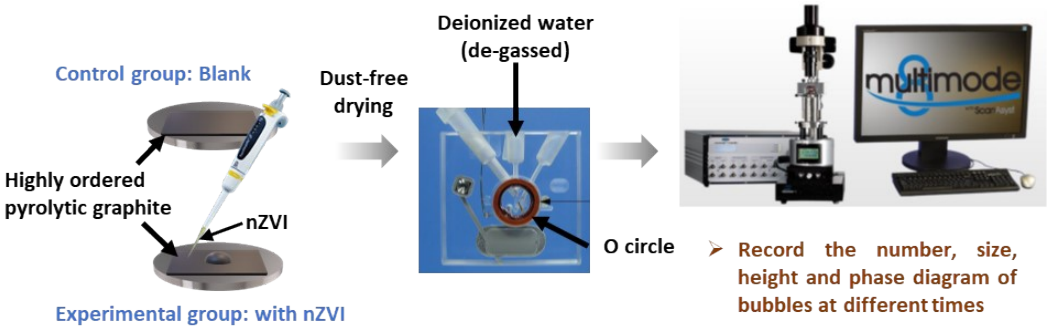

Figure S3. Schematic of in situ AFM imaging for monitoring nanobubble formation during nZVI corrosion.

Text S6. L-SEM workflow for early-Stage interfacial imaging

L-SEM was used to visualize early interfacial changes during the reaction of nZVI with water. Freshly prepared nZVI suspensions in ethanol (control) and DIW (experimental system) were loaded into a four-well stainless-steel liquid holder compatible with the SEM stage, following the same sample-loading procedure consistent with that used for STXM liquid-cell preparation to ensure comparable solution environments. Both the nZVI–C_2H_5OH and nZVI–H_2O systems were imaged under identical L-SEM conditions (EHT = 10.00 kV, WD = 9.7 mm, Signal A = BSD1; ZEISS GeminiSEM 300, Germany). L-SEM imaging enabled direct comparison of early-stage interfacial restructuring in the ethanol and aqueous systems during nZVI corrosion.

Text S7. Cyclic voltammetry

CV measurements were performed using an electrochemical workstation (CHI660D, Chenhua Instruments, Shanghai, China) with nZVI loaded onto carbon cloth as the working electrode. A conventional three-electrode configuration was employed in a 100 mL single-chamber sealed electrochemical cell, consisting of a platinum foil counter electrode and an Ag/AgCl reference electrode. Before each measurement, 60 mL of N_2-saturated Na_2SO_4 electrolyte solution (50 mM) was introduced into the cell. The potential was swept from different starting potentials (−1.0 to −1.2 V vs. Ag/AgCl) to a common final potential of 0.4 V, at a scan rate of 50 $mV \cdot s^{-1}$.

The working electrode was prepared as follows. The carbon cloth was cleaned by three sequential rinses with isopropanol and deionized water, followed by drying at 60 °C for 3 h. Freshly synthesized nZVI (5.0 mg) was dispersed in a mixed solution containing 0.2 mL isopropanol, 0.8 mL deionized water, and 10 μL Nafion, forming a homogeneous suspension. Under anaerobic conditions, 10 μL of the suspension was drop-cast onto the pretreated carbon cloth and dried at 25 °C for 1 h before use.

Text S8. Electron paramagnetic resonance

EPR spectroscopy was employed to detect reactive radical species. EPR spectra were recorded on a Bruker EMX spectrometer using 5,5-dimethyl-1-pyrroline N-oxide (DMPO) as the spin-trapping agent (X-band, 9.363 GHz; sweep width, 500 Gs; center field, 3390 Gs). For radical detection, three parallel experiments were conducted: (1) nZVI (100 $mg \cdot L^{-1}$) was reacted in N_2-purged deionized water under sealed, anaerobic conditions for 30 min, followed by the addition of DMPO and further reaction in a shaker. Samples were collected at 0, 1, 5, 10, and 30 min, filtered through 0.22 μm membranes, and subjected to EPR analysis; (2) a control experiment was performed under identical conditions except that N_2-purged ethanol was used as the solvent; (3) a blank test was conducted in N_2-purged deionized water without nZVI.

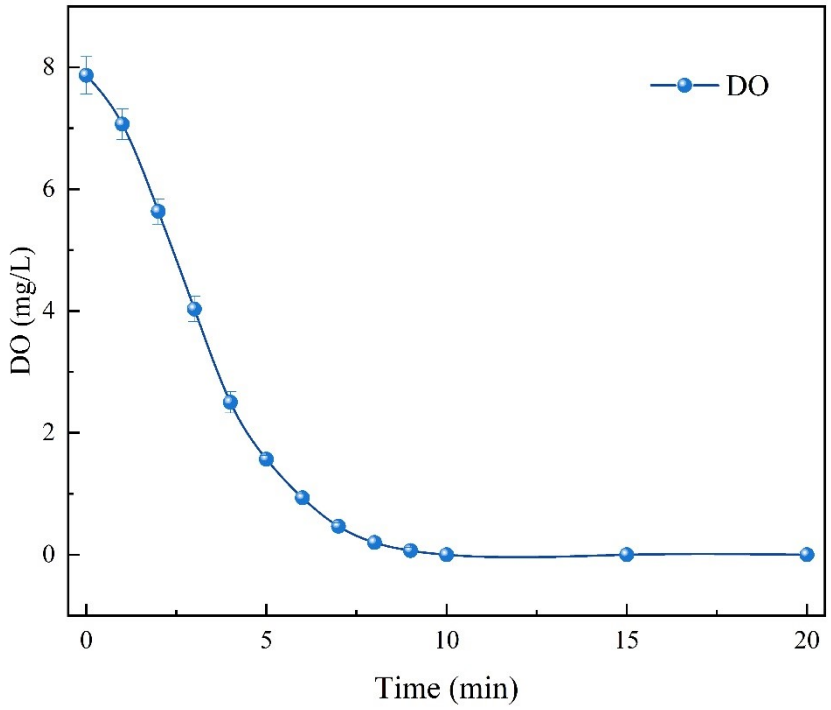

Figure S4. Time-dependent dissolved oxygen (DO) concentration during N_2 purging. Conditions: 200 mL DIW, purged with N_2 at a flow rate of 0.5 L min^{-1}. DO concentrations were monitored using a JPB-607A dissolved oxygen meter (INESA Scientific Instrument Co., Ltd., Shanghai, China). The DO level decreased rapidly and approached 0 mg L^{-1} within 10 min, confirming effective deoxygenation prior to anaerobic experiments.

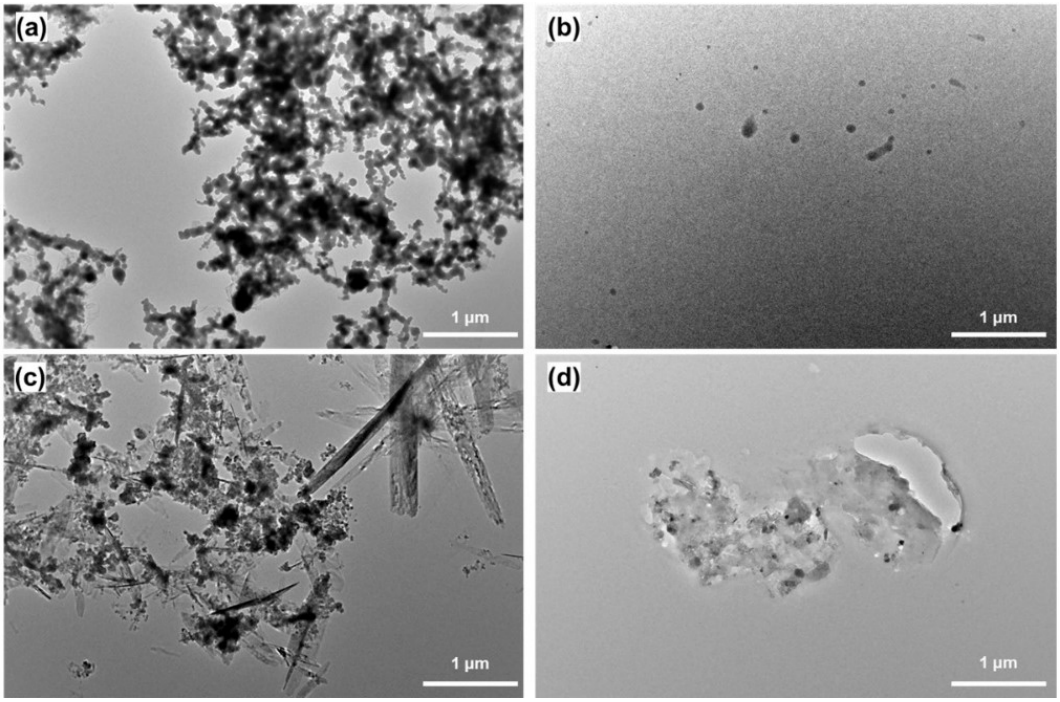

Figure S5. Effect of filtration on particle removal in the in solution (nZVI: 200 mg/L, reaction time: 48 h). (a) Unfiltered nZVI-C_2H_5OH system; (b) filtered nZVI-C_2H_5OH system;(c) unfiltered nZVI-H_2O system; (d) filtered nZVI-H_2O system.

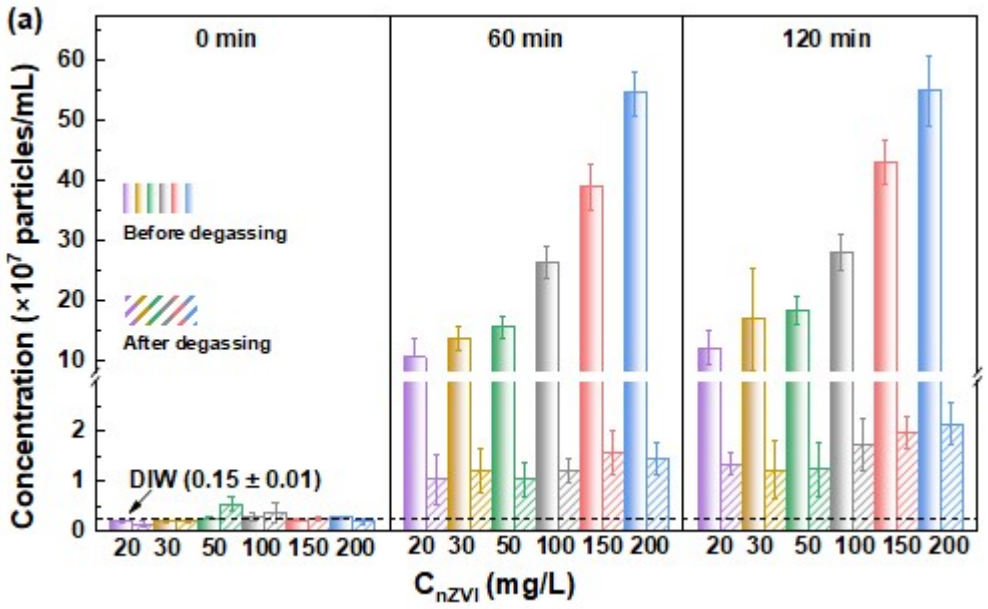

Figure S6. NTA quantification of hydrogen nanobubbles formed during aqueous nZVI corrosion. Number concentrations of nanoscale scatterers attributed to HNBs measured in 0.22 μm–filtered filtrates from the nZVI–H_2O system at nZVI loadings of 20, 30, 50, 100, 150 and 200 mg L^{-1} over 0–120 min, with N_2-aerated DIW (30 min) and an nZVI–ethanol suspension (0 min) included as controls. [7]

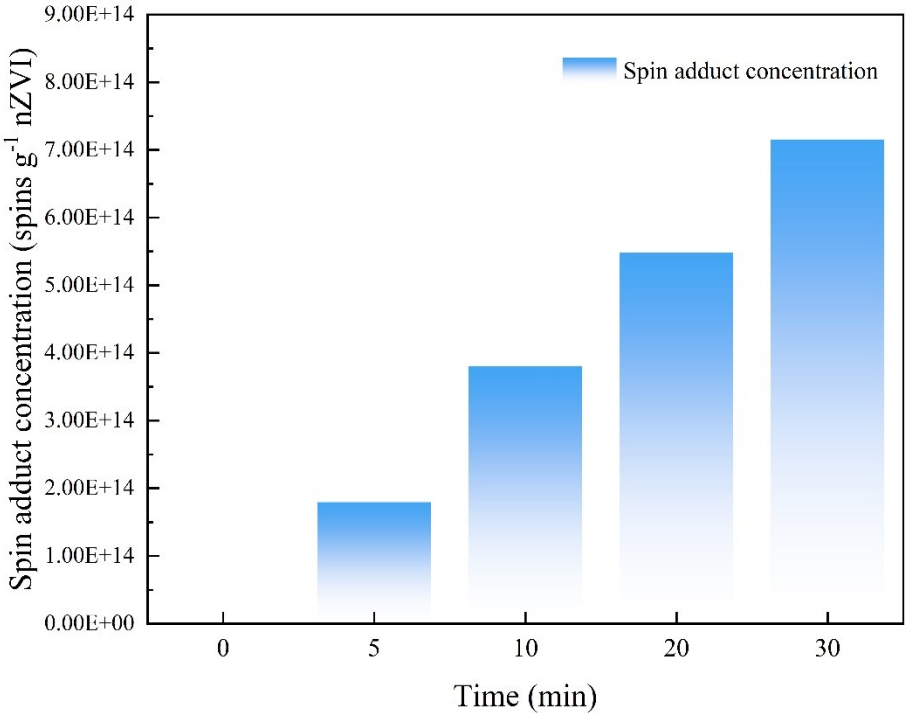

Figure S7. Time-dependent accumulated EPR spin concentration of hydrogen-associated paramagnetic intermediates in the nZVI–H_2O system.

References

1. S. Liu, J. Li, S. Oshita, M. Kamruzzaman, M. Cui and W. Fan, Acs Sustainable Chemistry & Engineering, 2021, 9, 11100-11109.
2. Y. Zhang, W. Fan, X. Li, W.-X. Wang and S. Liu, Environmental Science & Technology, 2022, 56, 15096-15107.
3. V. Filipe, A. Hawe and W. Jiskoot, Pharm Res, 2010, 27, 796-810.
4. L. Liang, W. Yang, X. Guan, J. Li, Z. Xu, J. Wu, Y. Huang and X. Zhang, Water Research, 2013, 47, 5846-5855.
5. J. Zhou, J. Wang, H. Liu, M. N. Banis, X. Sun and T.-K. Sham, Journal of Physical Chemistry Letters, 2010, 1, 1709-1713.
6. L. Wang, X. Wang, L. Wang, J. Hu, C. L. Wang, B. Zhao, X. Zhang, R. Tai, M. He, L. Chen and L. Zhang, Nanoscale, 2017, 9, 1078-1086.
7. Q. Huang, J. Qi, L. Zhou, Y. Wang, W. X. Zhang, J. Hu, R. Tai, S. Wang, A. Liu and L. Zhang, Environmental Science and Technology, 2024, 58, 4357-4367.